The effect of boron incorporation on leakage and wake-up in ferroelectric $Al_{1-x}Sc_xN$ EP

Maike Gremmel,[1,a)] Chandrashekhar Prakash Savant,[2] Debaditya Bhattacharya,[3] Georg Schönweger,[1,4]
Debdeep Jena,[2,3,5] and Simon Fichtner[1,4]

AFFILIATIONS

[1]Institute of Material Science, Kiel University, Kiel, Germany
[2]Department of Materials Science and Engineering, Cornell University, Ithaca, NY 14853, USA
[3]School of Electrical and Computer Engineering, Cornell University, Ithaca, NY 14853, USA
[4]Fraunhofer Institute for Silicon Technology (ISIT), Itzehoe, Germany
[5]Kavli Institute at Cornell for Nanoscale Science, Ithaca, NY 14853, USA

[a)]Author to whom correspondence should be addressed: magr@tf.uni-kiel.de

ABSTRACT

This study explores the influence of boron incorporation on the structural and electrical properties of ferroelectric aluminum scandium nitride ($Al_{1-x}Sc_xN$) thin films, focusing on leakage currents, wake-up effects, and imprint behavior. $Al_{1-x}Sc_xN$ films were incorporated with varying boron concentrations and analyzed under different deposition conditions to determine their structural integrity and ferroelectric performance. Key findings include a reduction in leakage currents, non-trivial alterations in bandgap energy, and an increasing coercive field with increasing boron content. Films with 6–13 at. % boron exhibited N-polar growth, while those with 16 at. % boron showed mixed polarity after deposition, which affected their ferroelectric response during the initial switching cycles—as did the addition of boron itself compared to pure $Al_{1-x}Sc_xN$. With increasing boron content, wake-up became gradually more pronounced and was strongest for pure $Al_{1-x}B_xN$.

I. INTRODUCTION

In recent years, the quest for innovative materials for microelectronic applications has intensified, driven by the need for reduced power consumption and increased functionality, while at the same time maintaining compatibility with existing technology platforms. Among these materials, piezo- and ferroelectric III-nitride based compounds have emerged as a promising contender, showcasing a plethora of positive attributes that position it as a promising emerging material in the field of microelectronics.[1–5]

The intrinsic characteristics of the wurtzite-type ferroelectrics, such as $Al_{1-x}Sc_xN$, make the material a compelling choice for numerous applications. Notably, it is lead-free, aligning with contemporary environmental standards and regulations. Its compatibility with complementary metal–oxide–semiconductor (CMOS) technology further enhances its appeal, facilitating seamless integration into existing electronic systems.[3,5–8]

One of the standout features of $Al_{1-x}Sc_xN$ is its high spontaneous polarization and high resistance to spontaneous depolarization, which make the material of interest for ferroelectric random access memory (FRAM).[1] Moreover, its exceptional temperature stability, good long-term stability, and chemical resilience underscore its reliability in demanding environments.[6] Furthermore, $Al_{1-x}Sc_xN$ boasts relatively low permittivity, contributing to its energy efficacy in various electronic and electromechanical applications.[7,9]

The combination of those properties in $Al_{1-x}Sc_xN$ open avenues for its utilization in cutting-edge technologies such as neuromorphic computing, ferroelectric memories, and micro-actuators and -sensors—in particular, if they are to be used in harsh environments.[10–12]

Despite numerous advantageous properties, $Al_{1-x}Sc_xN$ is not exempt from a few inherent drawbacks that can influence its

performance and reliability in the aforementioned applications. One notable drawback of $Al_{1-x}Sc_xN$ lies in its susceptibility to leakage due to the high coercive fields (E_c) that are required to invert its polarization (P).[13,14] This characteristic poses challenges, particularly for applications where the risk of electrical failure and leakage must be carefully managed to ensure device integrity and longevity. During the deposition process and device operation, another challenge arises as one polarization direction can become favored over the other. This leads to imprint, i.e., the coercive field for one polarity having a larger absolute value than for the other, that varies over time as well as wake-up, i.e., an increase in the switching polarization during the initial switching cycles.[15–19] This phenomenon can significantly complicate the operation of memory devices.

To address the drawbacks associated with $Al_{1-x}Sc_xN$, one promising approach is the incorporation of different materials through doping/alloying.[20] Incorporation of high bandgap compounds can potentially increase the bandgap of the alloy, thereby reducing leakage. Boron doping presents a particularly intriguing possibility, as $Al_{1-x}B_xN$ has been shown to be ferroelectric itself and the bandgap of w-BN (5.5–6.84 eV) is larger than the bandgap of $Al_{1-x}Sc_xN$ (4.7 eV at x = 0.30).[21–24] On the other hand, also the coercive field of $Al_{1-x}B_xN$ is higher than that of $Al_{1-x}Sc_xN$, which complicates switching it with on-chip voltage supplies and $Al_{1-x}B_xN$ might be more prone to feature wake-up.[2,18]

This work, therefore, determines whether the advantages of $Al_{1-x}Sc_xN$ and $Al_{1-x}B_xN$ can be combined by forming a quaternary solid solution of $Al_{1-x-y}B_xSc_yN$. The effect of doping $Al_{1-x}Sc_xN$ films with varying amounts of boron via co-sputtering is studied and complemented by structural and electrical analysis to evaluate film quality, boron content, lattice parameters, and other pertinent characteristics under different deposition conditions. We aim to investigate the impact of boron doping on key properties such as the coercive field, bandgap, leakage, and the initial imprint and wake-up.

II. MATERIALS AND METHODS

$Al_{1-x-y}B_xSc_yN$ films of 250 nm thickness with different boron concentrations were prepared on oxidized Si(100) wafers, which were covered with a 100 nm thick Pt bottom electrode. Al and Sc were co-sputtered with a constant power ratio of 680–320 W from DC sources using pulsed DC-mode while B was deposited simultaneously from an RF source with a power supply of 0 to 400 W. Unless stated otherwise, all samples were deposited with 7.5 SCCM Ar + 15 SCCM N_2 flow. All depositions were performed with single element targets (3N or better) in an Oerlikon MSQ 200 co-sputter system and a target–substrate distance of 100 mm. Different deposition temperatures with a fixed power supply of 400 W applied to the boron target were applied to tune the crystal quality and electrical properties. The specific experimental parameters are stated in Sec. III of this work. The boron content was measured using X-ray photoelectron spectroscopy (ThermoScientific NEXSA XPS). The surface was cleaned by Ar+ ion beam etching for 40 s and the average of five data points on the sample was used. For structural investigation, scanning electron microscopy (SEM) (Zeiss Gemini Ultra55) was used to determine the thickness of

the films as well as the homogeneity of the deposition (e.g., the presence of abnormally oriented grains, AOGs).[25] X-ray diffraction (XRD) (Rigaku SmartLab instrument, 9V,Cu) Θ–2Θ scans and ω rocking curves (RCs) were used to determine lattice parameters as well as crystal orientation. The lattice parameter c was determined by the 0002 $Al_{1-x}Sc_xN$ peak and a by in-plane measurements of the 1000 reflection (supplementary material, S2). For electrical characterizations, an additional Pt top electrode of 100 nm thickness was deposited *ex situ*, exposing the interfaces to oxidation (~5 nm). Standard lithography followed by ion beam etching was used to structure the top electrodes. Current density over electric field measurements (J–E) was performed using a triangular voltage signal (1.5 kHz if not stated otherwise) applied to the top electrode in an aixACCT TF Analyzer 2000 to determine coercive field and leakage current, respectively. The breakdown strength was extracted by increasing the applied electric field in multiple C–E measurements using the aixACCT TF Analyzer 2000 until an electric breakdown was induced (see Fig. S6 in the supplementary material). The capacitance (C) from which the relative permittivity (ε_r) was deduced and the loss tangent ($\tan\delta$) were determined using a Hewlett Packard 4284 A Precision LCR meter. The small signal voltage and frequency was set to 1 V and 100 kHz, respectively. Additionally, the bandgap of the different films was determined via Tauc fit from Ellipsometry (Fig. S1 in the supplementary material).

III. RESULTS AND DISCUSSION

A. Impact of growth temperature on film properties

Based on the structure zone model for sputter deposition, one of the main parameters influencing crystal growth is the deposition temperature. Therefore, growth temperatures between 300 and 500 °C were applied, using a fixed power of 400 W applied to the boron target and process gas flows of 7.5 SCCM Ar as well as 15 SCCM N_2 to study the structural and ferroelectric response of the $Al_{1-x-y}B_xSc_yN$ material. The aim was to determine process settings that result in films with good crystallinity and a uniform polarization direction over the wafer surface. The boron concentration for these $Al_{1-x-y}B_xSc_yN$ films is determined by XPS to be 16 at. %. Figure 1(a) shows symmetric XRD scans for $Al_{0.64}B_{0.16}Sc_{0.21}N$ films grown at different temperatures and that of an $Al_{0.75}Sc_{0.25}N$ film. With increasing deposition temperature, the lattice constant c of the $Al_{0.64}B_{0.16}Sc_{0.21}N$ films increases by 0.16 pm from 4.976 Å at 300 °C to 4.992 Å at 500 °C, indicating increasingly compressive in-plane stress [Fig. 1(b)]. Increasing the deposition temperature improves the XRD rocking curve-FWHM (full width at half maximum) of the 0002 $Al_{0.64}B_{0.16}Sc_{0.21}N$ reflection from 3.0° at 300 °C to 2.6° at 500 °C, indicating better crystal orientation. While depositions at 300 and 400 °C featured a certain amount of AOGs, 450 and 500 °C result in a homogeneous surface (and uniform grain size) as shown in Fig. 1(c). The $Al_{0.64}B_{0.16}Sc_{0.21}N$ films grown at higher substrate temperature have high crystallinity and fewer AOG.
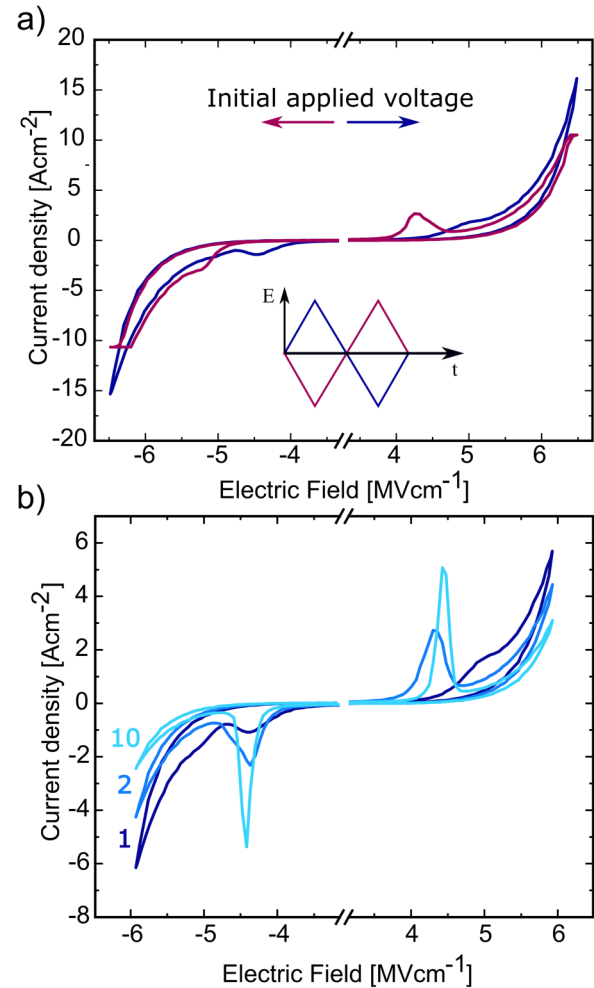
All samples exhibit ferroelectric behavior (Fig. S3 in the supplementary material). Textured wurtzite ferroelectrics like $Al_{1-x}Sc_xN$ can feature either nitrogen polarity (N-polarity, polarization pointing downward) or metal polarity (M-polarity, polarization pointing upward). While $Al_{1-x}Sc_xN$ grows exclusively N-polar
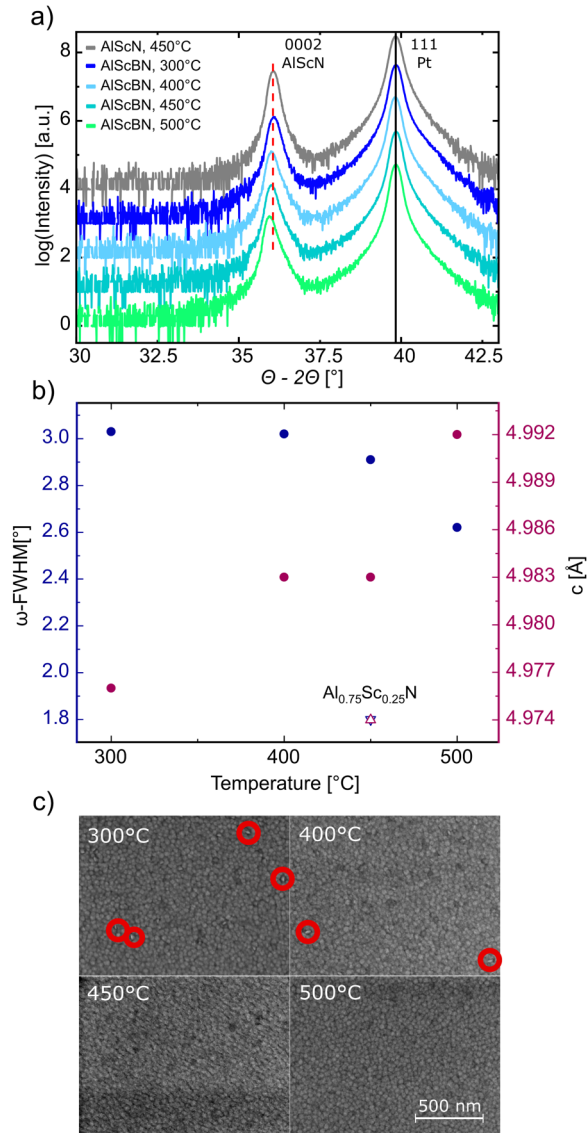
FIG. 1. (a) XRD Θ–2Θ scan for $Al_{0.64}B_{0.16}Sc_{0.21}N$ deposited at different temperatures compared to $Al_{0.75}Sc_{0.25}N$. (b) Full width at half maximum of the respective Rocking curves of 0002 reflections and the lattice parameter c. (c) Respective SEM images of $Al_{1-x-y}B_xSc_yN$ films at different deposition temperatures. AOGs are marked by red circles.

FIG. 2. $Al_{0.64}B_{0.16}Sc_{0.21}N$ deposited at 450 °C. (a) First cycle on pristine sample for negative voltage train vs positive applied voltage. (b) J–E peak formation from first to tenth cycle.

under the given process parameters, the boron-doped samples show displacement current peaks that result from ferroelectric switching for both electric field directions in the first cycle. Therefore, they feature mixed polarity after growth (Fig. 2). A notable change in the shape of the J–E curve is observed between the first and subsequent switching cycles, which manifests in the emergence of a switching current peak. In contrast, the first switching cycle features broad hysteresis areas at substantially larger

electric fields. This behavior can be interpreted such that $Al_{1-x}B_xN$ (unlike $Al_{1-x}Sc_xN$) starts to switch very inhomogeneously in terms of the electric field interval under which switching takes place. Nonetheless, it is able to recover the narrow electric field distribution characteristic of wurtzite ferroelectrics after a few cycles.

While N-polar $Al_{1-x}Sc_xN$ typically features negative imprint, $Al_{1-x-y}B_xSc_yN$ with mixed polarity shows a more symmetric hysteresis.[1,19]

As discussed previously, unipolar films initially lack pre-nucleated domains and/or low energy nuleation sites for the opposite polarity after deposition.[18,19] This asymmetry can facilitate an initial imprint. For mixed-polar samples, M-polar regions likely have a positive imprint, and N-polar regions have a negative one. This results in peak splitting/broadening, where one part of the volume switches at lower electric fields while the volume that was stabilized in opposite polarization direction during deposition switches at higher fields. During the

first switching of pristine samples, only the volume with the as-grown opposite polarity switches, requiring higher electric fields.

As $Al_{1-x}Sc_xN$ films with similar texture under similar process parameters are purely N-polar in its as-grown state, it can be suspected that the inclusion of boron itself leads to a stronger tendency for mixed-polar growth.
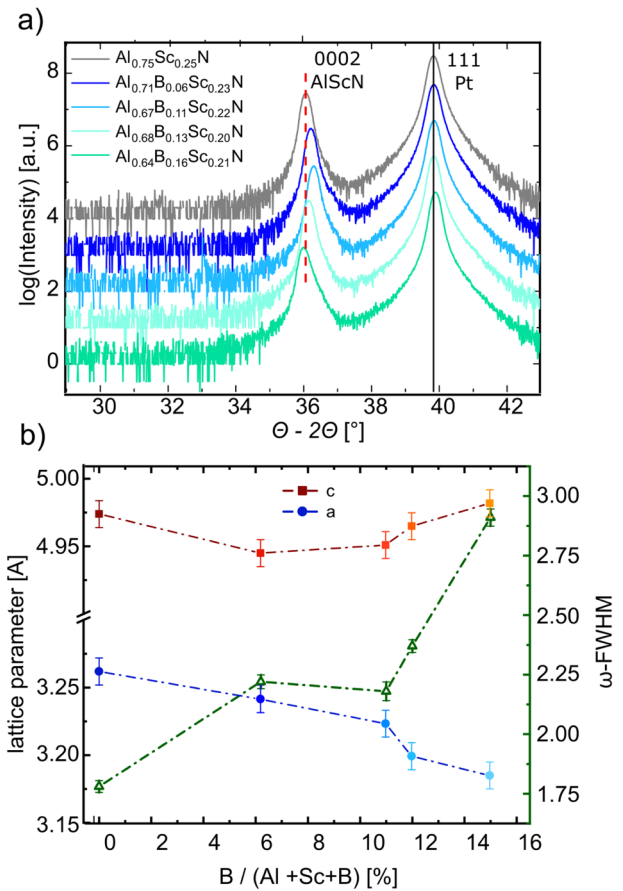
B. Influence of boron concentration on the structural properties

Next, the effect of boron concentration was investigated. Since 16 at. % is already close to the reported stability limit of $Al_{1-x-y}B_xSc_yN$, the variation in composition was directed toward less than 16 at. %.[2] For these depositions, a temperature of 450 °C was chosen, due to the improved 0002 rocking curve FWHM as well as comparability to existing sample sets of $Al_{1-x}Sc_xN$ without boron. To vary the boron content, the power to the RF source was set to 0, 200, and 300 W. Furthermore, one more sample was deposited at 400 W, 7.5 SCCM Ar, and 10 SCCM N_2, which turned out to re-stabilize exclusively N-polar growth at 13 at. % boron. To compare with the literature on $Al_{1-x}B_xN$, an additional $Al_{1-x}B_xN$ film without Sc was deposited with 1000 W applied to the Al target and 300 W to the boron target.

An overview of all depositions is listed in Table I together with the lattice parameters determined via XRD (Fig. S2 in the supplementary material). The atomic ratio Sc/(Al+Sc) determined via XPS remains unchanged at around 25% for all $Al_{1-x-y}B_xSc_yN$ thin films with boron concentrations in between 0 and 16 at. % ($x = 0$–0.16). The oxygen concentration is below 1.3%. In Θ–2Θ scans, an initial decrease in lattice parameter c is observed for $x = 0.06$ and 0.11 compared to $Al_{0.75}Sc_{0.25}N$, which then increases for $x = 0.13$ and 0.16. While c for $x = 0.13$ is still smaller than $Al_{0.75}Sc_{0.25}N$, for $x = 0.16$ it becomes larger (Fig. 3). The lattice parameter a becomes smaller with increasing x. The FWHM of a rocking curve scan around 0002, as listed in Table I, shows a slight decrease in crystal quality toward samples with higher x. $Al_{1-x-y}B_xSc_yN$ with $x = 0.06$, 0.11, and 0.13 demonstrate similar crystal qualities, as does $Al_{1-x}B_xN$, while the FWHM gets significantly larger for depositions at 400 W, but nonetheless stays below 3°. The c/a ratio increases upon boron incorporation and is highest for the $Al_{0.64}B_{0.16}Sc_{0.21}N$ sample, with 1.576 (Table I). This is contrary to observations on $Al_{1-x}B_xN$, where the c/a ratio stays constant at around 1.6.[2] The SEM surface images of all films deposited at 450 °C are free from AOGs [Fig. 4(b)].

FIG. 3. (a) XRD Θ–2Θ scan for different boron concentrations of $Al_{1-x-y}B_xSc_yN$ and (b) lattice parameters a, c and FWHM of the corresponding films.

TABLE I. Power applied to the boron target (P_B), N_2 flow, 0002 RC FWHM, and lattice constants of the various $Al_{1-x-y}B_xSc_yN$ samples.

P_B (W)	N_2 (SCCM)	B (at. %)	FWHM (°)	c (Å)	a (Å)	c/a
0	15	0 ± 0	1.78	4.98	3.26	1.52
200	15	6.2 ± 0.3	2.22	4.95	3.24	1.52
300	15	10.7 ± 0.2	2.18	4.95	3.22	1.53
300,0 (Sc)	15	…	2.15	5.08	3.18	1.59
400	15	15.5 ± 0.3	2.91	4.98	3.19	1.56
400	10	12.9 ± 0.2	2.37	4.96	3.20	1.57

C. Influence of boron concentration on the (ferro-) electric properties

Ellipsometry measurements (Fig. S1) show an initial increase in bandgap for increasing boron concentration in the films up to 11%, before it decreases back to similar values as $Al_{0.75}Sc_{0.25}N$. This is contrary to calculations and experimental data published on $Al_{1-x}B_xN$,[2] where an increase in boron leads to a reduced bandgap E_g—however, starting from the 6 eV of pure AlN,[26] compared to 5.17 eV of $Al_{0.75}Sc_{0.25}N$ from this work. The different behavior can be motivated by the higher bandgap of BN in comparison to ScN. As ScN reduces the bandgap of $Al_{1-x-y}B_xSc_yN$, BN apparently counteracts this effect as intended. As can be expected from a material with increased E_g, larger boron concentrations do increase the breakdown field E_{Bf} (Fig. S6 in the supplementary material). However, at the same time also E_c (Fig. 5) increases with increasing boron concentration, which is opposite to investigations on $Al_{1-x}B_xN$—yet again plausible considering the, in general, higher coercive field of $Al_{1-x}B_xN$ compared to $Al_{1-x}Sc_xN$.[2] Because of the more rapid increase of E_c,
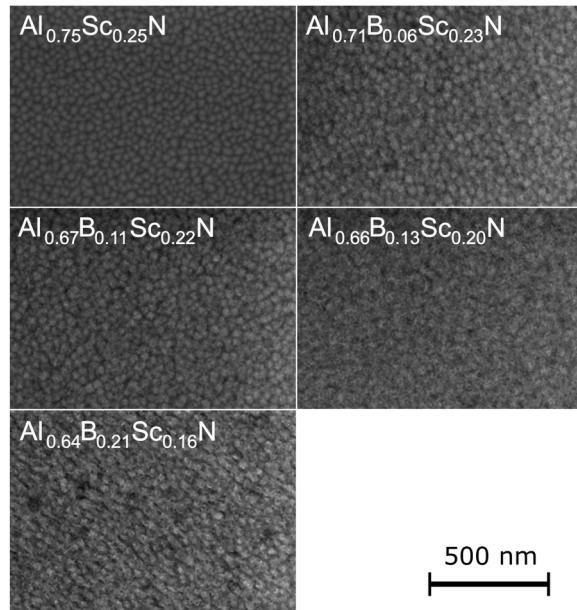
FIG. 4. SEM images of the various $Al_{1-x-y}B_xSc_yN$ surfaces.

FIG. 5. (a) $P-E$ hysteresis of $Al_{1-x-y}B_xSc_yN$ samples and (b) $E_c^{average} = (E_{c^+} + E_{c^-})/2$ vs boron concentration (after 100 cycles, 1.5 kHz) as well as c/a, ε_r and $\tan\delta$ vs boron concentration. All $P-E$ loops in a have their leakage current subtracted through peak fitting, as previously described.[19]

the ratio of breakdown voltage to E_c decreases for larger boron concentrations (all values are listed in Table II). However, there is a significant improvement in leakage currents compared to $Al_{1-x}Sc_xN$, even if the electric field is normalized to the respective E_c. This is shown in Fig. 6. Up to 13 at. % boron, the $Al_{1-x-y}B_xSc_yN$ films demonstrate a strong improvement of leakage with 6 at. % having an optimum of 80% reduction compared to $Al_{0.75}Sc_{0.25}N$. The 16% sample shows an improvement of leakage in M-polarity but gets worse for N-polarity. While the 16% B containing film is mixed polar, all other samples grow exclusively N-polar (Fig. S4 in the supplementary material). Overall, the reduction of leakage is consistent with the observed change in bandgap energy. The samples with higher bandgaps show a reduced leakage, while the $Al_{1-x-y}B_xSc_yN$ sample with the highest boron content and $Al_{0.75}Sc_{0.25}N$ feature a similar bandgap and leakage. The $J-E$ curves of which the leakage is extracted is included in the supplementary material (Fig. S5). In spite of the increasing coercive field, the relative permittivity ε_r is increasing as well, contrary to what is observed for $Al_{1-x}Sc_xN$.[25] The relative permittivity of the AlScN film was measured to be 18.85 at 0% B. The relative permittivity of the AlScBN films increases by increasing the B% to up to 21.79–22.14 for 13%–16% B. The B incorporation in the AlN is reported to increase its dielectric constant;[2] thus, an increase in dielectric constant of AlScBN film compared to AlN could be expected. However, with respect to the increasing coercive field with increasing B incorporation, the increase in dielectric constant is unexpected, as a higher E_c usually correlates to lower ε_r in ferroelectrics.[8]

In terms of remanent polarization, no clear trend toward higher or lower values with increasing boron concentration can be
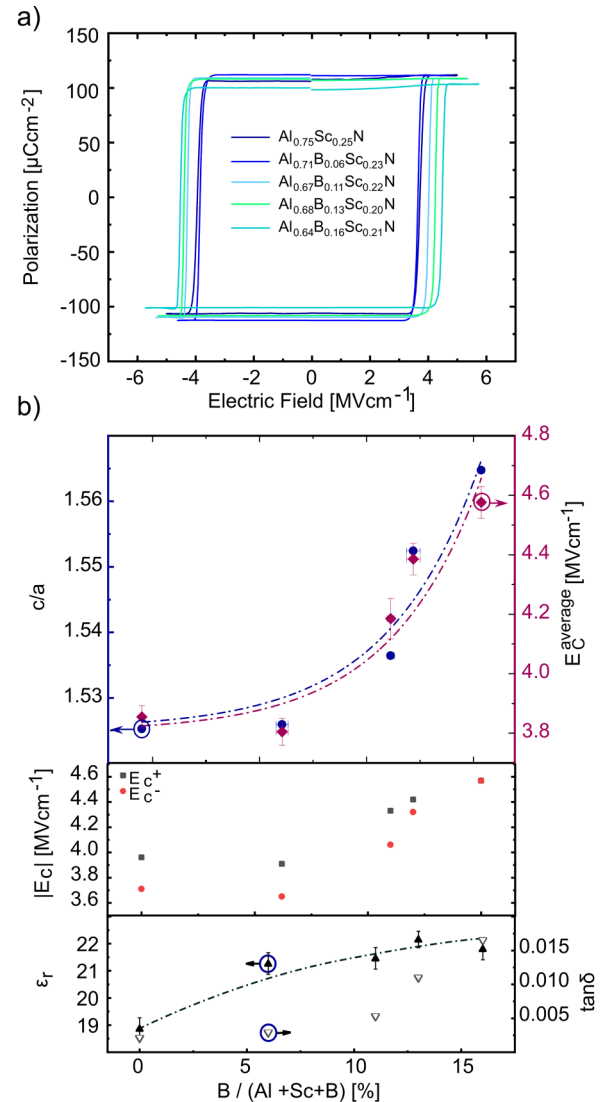
identified, which suggests the value and thus also the spontaneous polarization of the lattice is relatively independent of the investigated composition interval. For the pure $Al_{1-x}B_xN$ film, E_c is more than 3 MV cm^{-1} higher than for $Al_{1-x-y}B_xSc_yN$ deposited at the same target power [Fig. 7(c)]. For $Al_{1-x}B_xN$, Zhu et al. measured 6 MV cm^{-1} at 100 Hz on epitaxial films at lower B concentration.[18] To compare both values, the E_c at frequencies between 500 and 2500 Hz were extrapolated to determine E_c at 100 Hz (Fig. S7 in the supplementary material) (due to leakage, it was not possible to measure E_c directly at lower frequencies). With 7.28 MV cm^{-1} at

23 June 2025 13:11:24

TABLE II. Electrical characteristics of $Al_{1−x} − yB_xSc_yN$ thin films. The bandgap was determined via ellipsometry measurements. E_{Bf} and E_c were measured on pre-cycled capacitors (100 times) at 1.5 kHz. ε_r of as-grown capacitors were measured using a small signal frequency of 100 kHz and 1 V amplitude. Errors are estimated from the uncertainties in film thickness and capacitor area as well as from the standard deviation of the Tauc fit.

| B (at. %)	E_g (eV)	E_{Bf}/E_c	P_r (μC cm^{-2})	ε_r
0	5.17 ± 0.04	2.2 ± 0.1	109 ± 5	18.85 ± 0.4
6	5.23 ± 0.03	2.2 ± 0.1	112 ± 5	21.25 ± 0.4
11	5.26 ± 0.02	2.0 ± 0.1	104 ± 5	21.44 ± 0.4
13	5.19 ± 0.03	1.7 ± 0.1	108 ± 5	22.14 ± 0.4
16	5.16 ± 0.03	1.9 ± 0.1	106 ± 5	21.79 ± 0.4
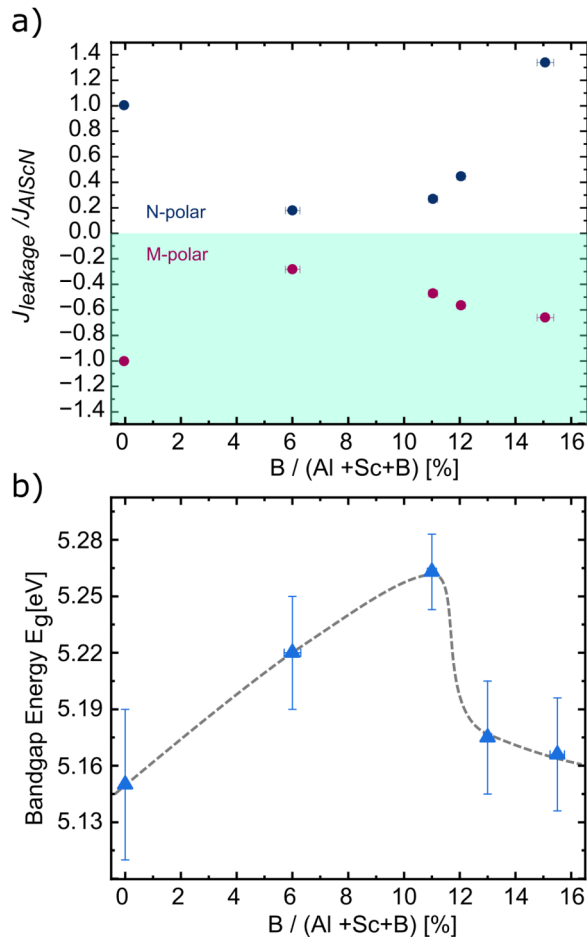
FIG. 6. (a) Leakage current $J_{leakage}$ normalized to leakage of $Al_{0.75}Sc_{0.25}N$ extracted from J–E curves that were themselves normalized to their respective E_c and (b) E_g vs boron concentration.

100 Hz, the E_c is still significantly higher than for the epitaxial film even though the coercive field of $Al_{1−x}B_xN$ was shown to decrease with higher B content.[2] Furthermore, compared to $Al_{1−x}Sc_xN$, where the full P_r can easily be switched in the first cycle, a distinct displacement current peak appears in the J–E curves only after several hundred cycles, resulting in the opening of the P–E hysteresis loops [Fig. 7(b)].

When plotting the normalized coercive fields extracted from the J–E measurements against the number of cycles, as shown in Fig. 7(a), it becomes evident that boron significantly impacts imprint and imprint shift during the first few switching cycle. The shift in negative E_c with cycling for $Al_{0.75}Sc_{0.25}N$ follows a logarithmic relationship, with all measurements aligning linearly on a logarithmic scale. With increasing boron content, the data deviate more from this logarithmic relationship, in particular, for the initial three switching cycles. For 13% boron, E_c shifts by 6% from the first to the second measurement while the shift of $Al_{0.75}Sc_{0.25}N$ is only 1.5%. This implies that the initial nucleation of oppositely polar domains appears to be energetically more costly in boron containing samples than in pure $Al_{1−x}Sc_xN$—a trend that continues as the boron concentration is increased.

The shift in positive E_c with cycling follows the logarithmic relationship from the start for both $Al_{0.75}Sc_{0.25}N$ and $Al_{1−x−y}B_xSc_yN$. However, the slope of the fit is significantly steeper for $Al_{1−x−y}B_xSc_yN$, indicating a more pronounced variation in imprint.

The results are a good indication that the increase in imprint upon boron incorporation is a factor that may explain why wake-up for $Al_{1−x}B_xN$ is discussed more frequently in literature than for $Al_{1−x}Sc_xN$.[18,27,28] As shown in previous work, the formation of inversion domains at the electrodes during cycling enables switching of the polarity at lower coercive fields, stabilizing the non-native polarity and resulting in a shift of the hysteresis toward more symmetric fields during the first few cycles. If the applied electric field amplitude is too small due to limited breakdown resistance, E_c falls outside the measurable range and the film switches partially in the first cycles. Due to the imprint shift, this volume increases in each cycle until E_c lies fully in the measured voltage range and full polarity is reached after several cycles. As discussed above, it is apparently energetically more costly to nucleate the opposite polarity in an as-deposited film when the boron content is increased. This results in a higher negative coercive field for originally N-polar samples and, thus, a higher chance to observe wake-up—which in our study was most pronounced for $Al_{1−x}B_xN$ without Sc incorporation. A potential explanation for the more pronounced wake-up effect in boron containing films lies in the change of polarization switching mechanisms influenced by the difference in chemical compositions. Lee et al.[29] proposed that in wurtzite-type ferroelectrics, polarization switching can proceed through various intermediate structures, with switching barriers predominantly governed by the more electronegative cations. For instance, $Al_{1−x}B_xN$ was predicted to favor such an individual switching pathway, whereas $Al_{1−x}Sc_xN$ at the given Sc concentrations might still favor switching through the layered hexognal structure. Therefore, the effects of Sc and B incorporation might not stack and, given their different switching pathways, could result in different nucleation behavior. This might result in

23 June 2025 13:11:24
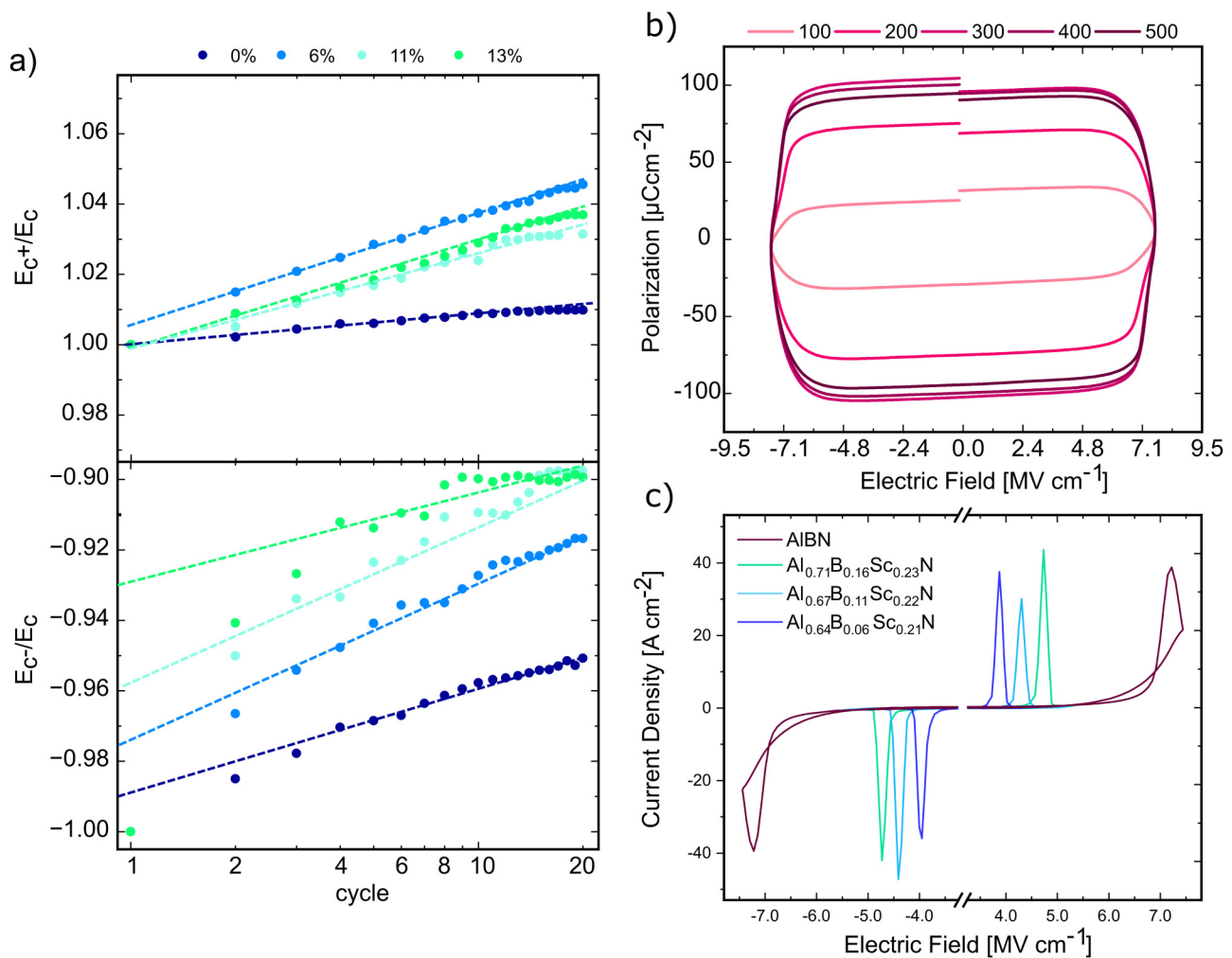
FIG. 7. (a) E_c of different $Al_{1-x-y}B_xSc_yN$ films over the number of cycles, (b) wake-up process of $Al_{1-x}B_xN$, and (c) comparison of J–E curves of different $Al_{1-x-y}B_xSc_yN$ films (100 cycles, 1.5 kHz) with $Al_{1-x}B_xN$ (>100 cycles, 1.5 kHz).

$Al_{1-x}B_xN$ requiring either more or larger nuclei for full polarization inversion than $Al_{1-x}Sc_xN$, thereby leading to a larger initial coercive field as well as a stronger change of the latter during the initial switching cycles. However, to fully elucidate the complex interplay between chemical composition, switching kinetics, and ferroelectric behavior in these materials, further investigations are necessary.

IV. CONCLUSION

This study investigated the impact of temperature and boron concentration on the structural and ferroelectric properties of $Al_{1-x-y}B_xSc_yN$ films. Higher temperatures lead to improved 0002 RC-FWHM values, indicating better crystallinity. Structural analyses via SEM also show a reduction in AOGs at elevated growth temperatures. Boron concentration notably affects the polarity of the films. Films with 6%–13% boron content exhibit N-polar

growth, while those with 16% boron show mixed polarity. This suggests that boron containing films might exhibit a higher tendency for M-polarity. With respect to the ferroelectric performance, the introduction of boron into $Al_{1-x}Sc_xN$ increases the coercive field and the breakdown strength, respectively; however, the E_c increases stronger than E_{Bf}. A significant change in ferroelectric properties from $Al_{1-x}Sc_xN$ over $Al_{1-x-y}B_xSc_yN$ to $Al_{1-x}B_xN$ is also evident from the increasing imprint shift with higher boron concentration. While the negative coercive field shifts by 1.5% in $Al_{0.75}Sc_{0.25}N$ in the first two cycles, it shifts by 6% for $Al_{1-x-y}B_xSc_yN$ with 13 at. % boron. The underlying tendency to require higher electric fields to switch the initial polarity provides an explanation for the more frequent occurrence of wake-up effects in $Al_{1-x}B_xN$ compared to $Al_{1-x}Sc_xN$. For leakage reduction, incorporating boron into $Al_{1-x}Sc_xN$ is shown to be beneficial and is correlated to E_g. Up to 13% boron, the $Al_{1-x-y}B_xSc_yN$

23 June 2025 13:11:24

films demonstrate a significant reduction in leakage currents compared to both $Al_{1-x}Sc_xN$ and $Al_{1-x}B_xN$. The reduction of leakage current is crucial for improving the performance and reliability of ferroelectric devices, making $Al_{1-x-y}B_xSc_yN$ films potentially advantageous for applications requiring low leakage currents.

SUPPLEMENTARY MATERIAL

See the supplementary material for additional information on electrical measurements, calculations of lattice parameters, and supporting graph for bandgap estimations by ellipsometry.

AUTHOR DECLARATIONS

Conflict of Interest

The authors have no conflicts to disclose.

Author Contributions

Maike Gremmel: Conceptualization (equal); Data curation (equal); Formal analysis (equal); Investigation (equal); Methodology (equal); Visualization (equal); Writing – original draft (equal); Writing - review & editing (lead). **Chandrashekhar Prakash Savant:** Data curation (supporting); Formal analysis (supporting); Investigation (supporting); Writing – review & editing (supporting). **Debaditya Bhattacharya:** Data curation (supporting); Formal analysis (supporting); Investigation (supporting); Writing – review & editing (supporting). **Georg Schönweger:** Data curation (supporting); Formal analysis (supporting); Investigation (supporting); Writing – original draft (supporting); Writing – review & editing (supporting). **Debdeep Jena:** Data curation (supporting); Formal analysis (supporting); Funding acquisition (supporting); Project administration (supporting); Resources (supporting); Supervision (supporting); Writing – review & editing (supporting). **Simon Fichtner:** Conceptualization (equal); Funding acquisition (lead); Investigation (supporting); Project administration (lead); Resources (lead); Supervision (lead); Validation (lead); Writing – original draft (supporting); Writing – review & editing (supporting).

DATA AVAILABILITY

The data that support the findings of this study are available from the corresponding author upon reasonable request.

REFERENCES

[1]S. Fichtner, N. Wolff, F. Lofink, L. Kienle, and B. Wagner, J. Appl. Phys. **125**, 114103 (2019).

[2]J. Hayden, M. D. Hossain, Y. Xiong, K. Ferri, W. Zhu, M. V. Imperatore, N. Giebink, S. Trolier-McKinstry, I. Dabo, and J.-P. Maria, Phys. Rev. Mater. **5**, 44412 (2021).

[3]P. Wang, D. Wang, S. Mondal, M. Hu, J. Liu, and Z. Mi, Semicond. Sci. Technol. **38**, 043002 (2023).

[4]M. Uehara, R. Mizutani, S. Yasuoka, T. Shiraishi, T. Shimizu, H. Yamada, M. Akiyama, and H. Funakubo, Appl. Phys. Lett. **119**, 172901 (2021).

[5]K. H. Kim, I. Karpov, R. H. Olsson, and D. Jariwala, Nat. Nanotechnol. **18**, 422 (2023).

[6]M. R. Islam, N. Wolff, M. Yassine, G. Schönweger, B. Christian, H. Kohlstedt, O. Ambacher, F. Lofink, L. Kienle, and S. Fichtner, Appl. Phys. Lett. **118**, 232905 (2021).

[7]S. Fichtner, G. Schönweger, F. Dietz, H. Hanssen, H. Züge, T.-N. Kreutzer, F. Lofink, H. Kohlstedt, H. Kapels, and M. Mensing, in *IEEE EDTM* (IEEE, 2023).

[8]T. Mikolajick, S. Slesazeck, H. Mulaosmanovic, M. H. Park, S. Fichtner, P. D. Lomenzo, M. Hoffmann, and U. Schroeder, J. Appl. Phys. **129**, 100901 (2021).

[9]G. Schönweger, A. Petraru, M. R. Islam, N. Wolff, B. Haas, A. Hammud, C. Koch, L. Kienle, H. Kohlstedt, and S. Fichtner, Adv. Funct. Mater. **32**, 2109632 (2022).

[10]R. Bez and A. Pirovano, Mater. Sci. Semicond. Process. **7**, 349 (2004).

[11]B. W. Wessels, Annu. Rev. Mater. Res. **37**, 659 (2007).

[12]A. I. Khan, A. Keshavarzi, and S. Datta, Nat. Electron. **3**, 588 (2020).

[13]L. Chen, Z. Wang, C. Liu, M. Li, W. Song, W. Wang, B. Varghese, H. K. Lee, H. Lin, and Y. Zhu, in *2023 IEEE International Symposium on Applications of Ferroelectrics (ISAF)* (IEEE, 2023), pp. 1–3.

[14]W. Yang, L. Chen, M. Li, F. Liu, X. Liu, C. Liu, and J. Kang, Appl. Phys. Lett. **123**, 132903 (2023).

[15]T. Schenk, M. Hoffmann, J. Ocker, M. Pešić, T. Mikolajick, and U. Schroeder, ACS Appl. Mater. Interfaces **7**, 20224 (2015).

[16]Y. Zhou, H. K. Chan, C. H. Lam, and F. G. Shin, J. Appl. Phys. **98**, 024111 (2005).

[17]M. Grossmann, O. Lohse, D. Bolten, U. Boettger, T. Schneller, and R. Waser, J. Appl. Phys. **92**, 2680 (2002).

[18]W. Zhu, F. He, J. Hayden, Z. Fan, J. I. Yang, J. Maria, and S. Trolier-McKinstry, Adv. Electron. Mater. **8**, 1 (2022).

[19]M. Gremmel and S. Fichtner, J. Appl. Phys. **135**, 204101 (2024).

[20]R. Kudrawiec and D. Hommel, Appl. Phys. Rev. **7**, 1 (2020).

[21]M. Levinshtein, S. Rumyantsev, and M. Shur, *Properties of Advanced Semiconductor Materials: GaN, AIN, InN, BN, SiC, SiGe* (John Wiley & Sons, 2001), p. 69.

[22]M. Baeumler, Y. Lu, N. Kurz, L. Kirste, M. Prescher, T. Christoph, J. Wagner, A. Zukauskaite, and O. Ambacher, J. Appl. Phys. **126**, 045715 (2019).

[23]M. Zhang and X. Li, Phys. Status Solidi B **254**, 1600749 (2017).

[24]J. X. Shen, D. Wickramaratne, and C. G. Van De Walle, Phys. Rev. Mater. **1**, 065001 (2017).

[25]S. Fichtner, N. Wolff, G. Krishnamurthy, A. Petraru, S. Bohse, F. Lofink, S. Chemnitz, H. Kohlstedt, L. Kienle, and B. Wagner, J. Appl. Phys. **122**, 035301 (2017).

[26]M. Feneberg, R. A. Leute, B. Neuschl, K. Thonke, and M. Bickermann, Phys. Rev. B: Condens. Matter Mater. Phys. **82**, 094417 (2010).

[27]K. Yazawa, D. Drury, J. Hayden, J. P. Maria, S. Trolier-McKinstry, A. Zakutayev, and G. L. Brennecka, J. Am. Ceram. Soc. **107**, 1523–1532 (2024).

[28]K. Yazawa, J. Hayden, J. P. Maria, W. Zhu, S. Trolier-McKinstry, A. Zakutayev, and G. L. Brennecka, Mater. Horiz. **10**, 2936 (2023).

[29]C.-W. Lee, K. Yazawa, A. Zakutayev, G. L. Brennecka, and P. Gorai, Sci. Adv. **10**(20), eadl0848 (2024).

23 June 2025 13:11:24